sustainability

MDPI

Article

Physical-Mechanical and Electrical Resistivity Properties of Cementitious Mortars Containing Fe_3O_4-MWCNTs Nanocomposite

Veyis Selen [1], Omer Guler [2], Mehrab Nodehi [3], Ahmet Sarı [4,5], Ali Yaras [6], Osman Gencel [7,*], Aliakbar Gholampour [8] and Togay Ozbakkaloglu [9,*]

[1] Department of Bioengineering, Firat University, 23119 Elazig, Turkey; vselen@firat.edu.tr
[2] Rare Earth Elements Application and Research Center, Munzur University, 62000 Tunceli, Turkey; oguler@firat.edu.tr
[3] Department of Civil Engineering, University of California, Davis, CA 95616, USA; mnodehi@ucdavis.edu
[4] Department of Metallurgical and Material Engineering, Karadeniz Technical University, 61080 Trabzon, Turkey; ahmet.sari@ktu.edu.tr
[5] Interdisciplinary Research Center of Renewable Energy and Power Systems (IRC-REPS), King Fahd University of Petroleum & Minerals, Dhahran 31261, Saudi Arabia
[6] Department of Metallurgical and Materials Engineering, Faculty of Engineering, Architecture and Design, Bartin University, 74110 Bartin, Turkey; aliyaras@bartin.edu.tr
[7] Civil Engineering Department, Faculty of Engineering, Architecture and Design, Bartin University, 74100 Bartin, Turkey
[8] College of Science and Engineering, Flinders University, Adelaide, SA 5042, Australia; aliakbar.gholampour@flinders.edu.au
[9] Ingram School of Engineering, Texas State University, San Marcos, TX 78666, USA
* Correspondence: ogencel@bartin.edu.tr (O.G.); togay.oz@txstate.edu (T.O.)

Abstract: Recent growth in materials science and engineering technologies has pushed the construction industry to engage in new applications, such as the manufacturing of smart and electrically conductive products. Such novel uses of conductive construction materials would potentially allow their use in conjunction with various fields, such as those referred to as "Industry 4.0." The following study uses iron oxide (Fe_3O_4)-multi-walled carbon nanotubes (MWCNTs) nanocomposites synthesized by chemical vapor deposition (CVD) and incorporated into the cementitious mortars as a substitute for sand at 1, 2, and 3% ratios to enhance the electrical conductivity. Results reveal that the electrical resistivity of cementitious composites decreases (due to the increase in electrical conductivity) from 208.3 to 61.6 Ω·m with both the Fe_3O_4-MWCNTs nanocomposites ratio and the increasing voltage. The lowest compressive strengths at 7 and 28 days are 12.6 and 17.4 MPa for specimens with 3% Fe_3O_4-MWCNTs and meet the standards that comply with most applications. On the other hand, the highest porosity was reached at 26.8% with a Fe_3O_4-MWCNTs rate of 3%. This increase in porosity caused a decrease in both the dry unit weight and ultrasonic pulse velocity (from 5156 to 4361 m/s). Further, it is found that the incorporation of Fe_3O_4-MWCNT nanocomposites can have a negative effect on the hardening process of mortars, leading to localized air cavities and an inhomogeneous development of cementing products. Nonetheless, the improvement of the electrical conductivity of the samples without significantly compromising their physico-mechanical properties will allow their use in various fields, such as deicing applications with low-voltage electric current.

Keywords: electrically conductive mortars; chemical vapor deposition (CVD); multi-walled carbon nanotubes (MWCNTs); iron oxide (Fe_3O_4); characterization

check for updates

Citation: Selen, V.; Guler, O.; Nodehi, M.; Sarı, A.; Yaras, A.; Gencel, O.; Gholampour, A.; Ozbakkaloglu, T. Physical-Mechanical and Electrical Resistivity Properties of Cementitious Mortars Containing Fe_3O_4-MWCNTs Nanocomposite. *Sustainability* **2023**, *15*, 11045. https://doi.org/10.3390/su151411045

Academic Editor: Miguel Bravo

Received: 2 June 2023
Revised: 30 June 2023
Accepted: 12 July 2023
Published: 14 July 2023

Copyright: © 2023 by the authors. Licensee MDPI, Basel, Switzerland. This article is an open access article distributed under the terms and conditions of the Creative Commons Attribution (CC BY) license (https://creativecommons.org/licenses/by/4.0/).

1. Introduction

Recent advances in the smartification and electrification of urban areas have increased the need for the production and use of high-performance composite materials. One of

the most recent advances in high-performance composites is the use of nano-designed composite cementitious materials with innovative uses, such as magnetic and conductive concrete, applicable for road electrification, electromagnetic shielding, and even energy harvesting processes [1,2]. Although the basic understanding of electromagnetism started as early as the 17th century, its actual application in materials science and other engineering fields has been arguably a slow but steady process. In general, "electromagnetism" refers to the type of physical interaction that takes place between electrically charged particles [3]. The most common form of magnetic effect can be seen in ferromagnetic materials, such as iron, nickel, and cobalt, and in a few rare-earth materials, such as neodymium, which are regarded as having the potential to be magnetized permanently [4,5]. As a result, due to the excellent electromagnetic wave absorption properties of certain nanomaterials, such as nano iron oxide (Fe_3O_4) [6], they have a considerable potential to be used in concrete, resulting in the production of sustainable composites.

There are, however, other nanomaterials that can be used for this purpose. Carbon nanotubes (CNTs), for instance, are nanostructured carbon-based materials that have an extremely high elastic modulus and excellent thermo-mechanical properties [7–11]. They are also known to be the strongest fibers for reinforcement purposes in composites [12] and to be magnetizable [13]. CNTs are commonly formed by rolling sheets of hexagonal carbon rings into hollow cylinders [7] and have a very low density of 1.75 g/cm^3 as well as an extraordinary thermal conductivity of 6000 W/m.K. compared to 385 W/m.K. of copper [14]. Nonetheless, to increase the physico-mechanical properties of this already impressive material, multi-walled carbon nanotubes (MWCNTs) are also produced, which can be thought of as multiple concentric rolled layers of carbon atoms. In general, single-walled carbon nanotubes (SWCNTs) and MWCNTs have a typical length of 0.8–2 nm and 5–20 nm, respectively [15]. Due to their superior properties, the incorporation of CNTs (in both the form of SWCNTs and MWCNTs) as reinforcing agents for polymers, ceramics, and metals has become an essential part of producing lightweight and high-performance nanocomposites [7,12]. Such innovative uses of nanocomposites are often regarded as sustainable composites [16,17]. Nonetheless, although CNTs have significantly high mechanical properties, their production and synthesis are often regarded as difficult processes [7,8].

To synthesize CNTs, laser ablation, hydrothermal (sono-chemical), arc discharge, electrolysis, and various forms of chemical vapor deposition (CVD) are most commonly practiced [8,18]. Despite the benefits of each synthesis technique, the CVD process is reported to have a higher yield and purity in producing CNTs [19] and be the most widely used, inexpensive method that can be commercially practiced [18–20]. This is due to the relatively lower pressure and temperature required in the CVD process compared to those of other methods, which makes CVD a cost-effective means for the production of high-purity semiconducting films at a considerably high deposition rate [7,8]. In general, CVD is a method that utilizes thermally induced chemical reactions in a vacuum at the surface of a substrate with reagents supplied in gaseous form. The CVD process is commonly divided into thermal, plasma, and laser groups that can activate the chemical reaction. Thermal CVD, for instance, functions by heating infrared radiation that leads to the decomposition of gases. A good case in point is the quartz tube reactor enclosed in a high-temperature furnace, as discussed in references [7,20]. In this method, a metal catalyst is initially deposited on the substrate, loaded into a CVD reactor, and then treated with a gaseous agent (e.g., ammonia) at high temperatures (commonly 750–950 °C). This results in the formation of nanometal particles on the surface of the substrate. Hydrocarbon gases are then added to the quartz tube reactor, which leads to the decomposition and diffusion of carbon atoms through metallic particles. This can further lead to the production of CNTs when the solution becomes supersaturated [7,8].

In general, although there are many uses for magnetized materials in electrical engineering, medical materials, and even astronautical sciences, their use in construction is still rather limited. Most specifically, in concrete technology, the use of magnetized

materials is an applicable practice in the production of self-sensing and smart concrete pavement [21], electromagnetic shielding [22], void detection [23], electrical curing [24], and Wi-Fi charging of moving vehicles [1]. In doing so, the most commonly used conductive materials (e.g., nanomaterials [25]) of various forms are utilized in concrete mixtures to increase the conductivity of this composite material. For instance, Chuewangkam et al. [26] utilized nano-size neodymium magnet (NdFeB) powder in the cement paste to produce a magnetic composite. They reported that the mechanical properties of the paste produced with magnetic powder were enhanced due to the increased density of the cement composite. He et al. [27] utilized nano-Fe_3O_4 magnetic fluid to produce an electromagnetic wave-absorbing cement-based composite with applications in the construction of electromagnetic wave interference shielding buildings. In their analyses, they found that the inclusion of magnetized fluid enhanced the nanoparticle dispersion and early hydration of the composite. Ahmed [25] used nanoalumina in water as magnetized water and reported enhanced physico-mechanical properties of concrete due to the internal magnetic force. Jiao et al. [6] utilized magnetized Fe_3O_4 to achieve active rheology control in combination with exposure to an external magnetic field that would enhance the dispersion and orientation of materials, especially steel fibers, within the fresh cement paste. In their analyses, they found that the effect of the magnetic field was more significant on the stiffening of the mixture than the size or content of Fe_3O_4 [6].

In light of the above information, it is clear that Fe_3O_4 structures have short diffusion distances for electrolyte ions and good tolerance to volume changes during electrochemical reactions. On the other hand, the use of Fe_3O_4 together with carbon nanotubes facilitates redox reactions and increases the use of Fe_3O_4 in electrochemical reactions. Therefore, electrical conductivity can be improved while reducing the electrical resistivity of Fe_3O_4-MWCNT nanocomposite prepared by integrating Fe_3O_4 structures into MWCNTs. Based on the literature review, although the existing studies evaluated the properties of concrete through the use of nanomaterials, none of them have reported the effect of Fe_3O_4-impregnated MWCNTs. The reason for utilizing Fe_3O_4-MWCNT nanocomposites is the numerous applications discussed in previous studies (e.g., [28]). Among the many, Fe_3O_4-MWCNTs nanocomposites can be used in concrete to improve the electrical conductivity of cement composites and thus dissolve the icing that occurs on the concrete surface in cold regions with low-voltage electric current. Based on the above-mentioned research gap, in this study, by using the CVD technique and sequential steps, the Fe_3O_4-MWCNTs nanocomposites are synthesized and then incorporated into a mortar and compared to ordinary mortars in terms of physico-mechanical, microstructural, and electrical conductivity properties. The following sections further elaborate on the experimental program conducted in this study.

2. Experimental Program

2.1. Materials

2.1.1. Ordinary Portland Cement

For this study, type I Portland cement conforming to ASTM C150 [29] with a specific gravity of 3.15 kg/m^3 was used. Further information on the physico-chemical properties of the cement is presented in Table 1.

Table 1. Chemical composition, setting time, specific gravity, and fineness of Portland cement used in this study.

SiO_2 (%)	18.8
Al_2O_3 (%)	5.3
Fe_2O_3 (%)	3.4
CaO (%)	63.7
MgO (%)	1.7
SO_3 (%)	2.7
$Na_2O_{(eqv)}$ (%)	0.8

Table 1. *Cont.*

Specific gravity	3.15
Setting time (Initial/Final)	165/205
Blaine fineness (m^2/kg)	333
Loss on ignition (LOI)	<4%
Setting time	>45 min (initial) and <6.5 h (final).

2.1.2. Aggregate

In this study, locally available limestone sand with a maximum size of 4.75 mm and a specific gravity of 1.64 was used. The particle size distribution of the sand used in this study is shown in Figure 1.

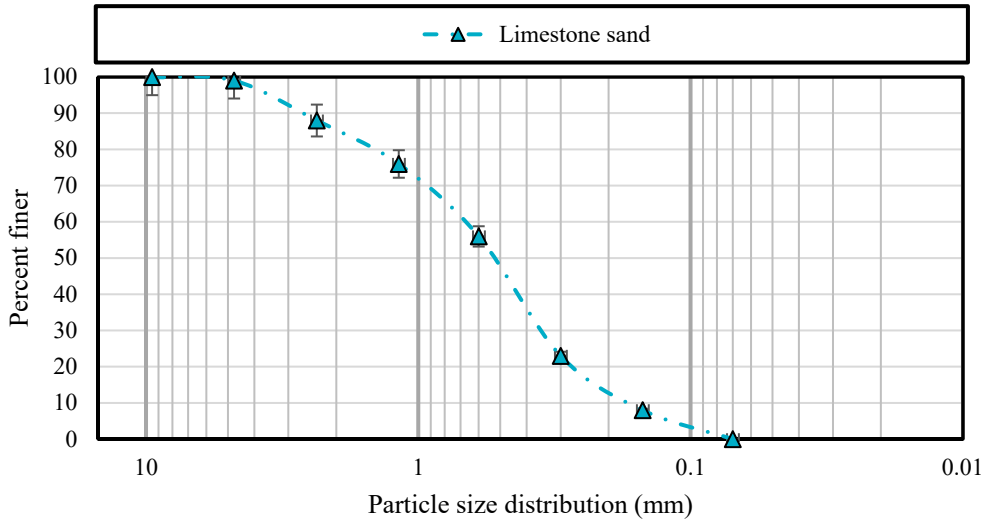

Figure 1. Sieve analysis conducted on limestone sand.

2.2. Synthesis of MWCNTs and Fe_3O_4-MWCNTs

In this study, CNTs were grown on p-doped Si (100) substrates, as recommended by Ref. [30] for enhanced radial growth of MWCNTs, and were further rinsed sequentially in acetone and ethanol in an ultrasonic bath before being vacuum filtered. This is due to the better dispersion of CNTs through ultrasonication compared to other methods, as discussed in Ref. [31]. Further, to ensure high efficiency, the size of Fe particles was reduced to nano-size in a ball mill, and they were distributed on a Si wafer to act as a transition metal catalyst. The reason for the use of a catalyst is the enhanced decomposition of the carbon source through elevated temperatures, as practiced in this study, or irradiation (plasma CVD), as discussed in Ref. [32].

The prepared substrates were placed at the center of the quartz tube reactor inside the furnace. The reason for utilizing the quartz tube reactor is the low solubility of CNTs in water [33,34]. Further, the tube was evacuated at a base pressure of 103 Torr by a rotative pump for purging. The furnace was then heated up to 650 °C under 2 Torr pressure in an argon (Ar) gas atmosphere (1 L/min.), as advised in the previous study that an argon environment can enhance the growth conditions of CNTs [18]. After 40 min, the furnace was left to cool in an Ar atmosphere. The produced powder was kept in a nitric acid/hydrochloric acid mixture with a ratio of 1:1 for 3 h to remove the amorphous carbon structures of the powder. Then, the powder was washed with distilled water and dried in an oven at 150 °C for 10 h. To characterize the powdered Fe3O4-MWCNTs, a series of X-ray diffraction analysis (XRD), fourier-transform infrared spectroscopy (FTIR), high-resolution transmission electron microscopy (HR-TEM), scanning electron microscope (SEM), and energy dispersive spectroscopy (EDS) tests were conducted. In this regard, the phase analysis and surface morphologies of the synthesized CNTs were characterized by XRD Bruker Advance D8, CuK, and HR-TEM Jeol Jem 2100F, respectively.

In this study, initially, MWCNTs were kept under an inert atmosphere in a muffle furnace at 350 °C for 30 min. MWCNTs were kept in an ultrasonic bath with concentrated nitric acid (HNO_3, 65%) for 100 min, washed with distilled water until a pH of ~7 was achieved, and then dried in a vacuum oven at 60 °C. Fe_3O_4-MWCNTs were synthesized based on chemical reactions of Equations (1) and (2) [35].

$$FeCl_2 \cdot 4H_2O + 2FeCl_3 \cdot 6H_2O + 8NH_4OH \rightarrow Fe_3O_{4(liquid)} + 8NH_4Cl + 20H_2O \quad (1)$$

$$Fe_3O_4 + MWCNT + 20H_2O \rightarrow Fe_3O_4 - MWCNT_{(liquid)} \quad (2)$$

The synthesis of Fe_3O_4-MWCNTs was carried out in a 500 mL three-necked glass flask in a water bath at 80 °C. $FeCl_2 \cdot 4H_2O$ and $FeCl_3 \cdot 6H_2O$ (1:2) were added to 200 mL of distilled water and the mixture was vigorously stirred with a mechanical stirrer to dissolve the ferric chlorides. Chemical reactions were carried out in nitrogen atmosphere and reflux was used to prevent heat loss due to evaporation. MWCNTs were added to the mixture consisting of iron salts (4:1 w/w), then the mixture was stirred for 10 min. Further, approximately 30 mL of 25% NH_4OH was slowly added to the mixture at 80 °C, so that the pH was 11–12. Stirring was continued for 30 min for the nanocomposite to complete its growth. The mixture was then cooled to room temperature to remove unreacted reactants at the end of the reaction and then washed with distilled water until pH of ~7. The synthesized Fe_3O_4-MWCNTs were separated from the solution using a neodymium magnet and then dried in a vacuum oven at 60 °C. The dried Fe_3O_4-MWCNTs were stored in a capped glass bottle to be used in further experiments. The flow diagram of Fe_3O_4-MWCNTs synthesis is given in Figure 2a. Figure 2b shows the synthesized Fe_3O_4-MWCNTs and Figure 2c presents the produced mortar specimens.

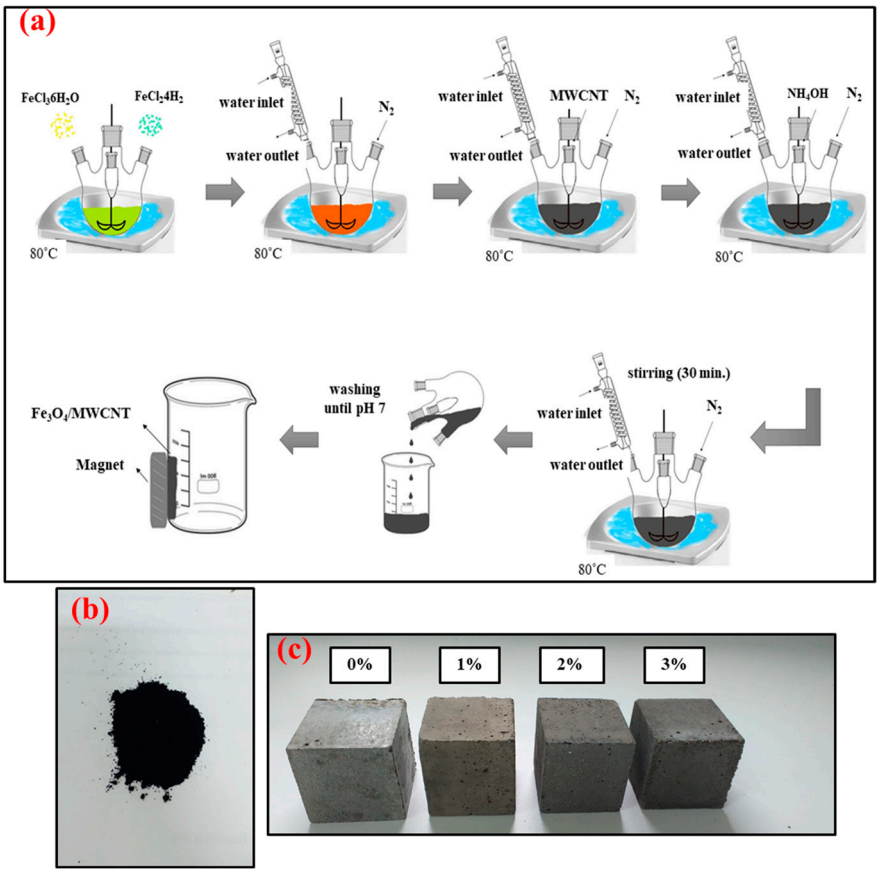

Figure 2. Diagram of Fe_3O_4-MWCNTs synthesis (**a**), synthesized Fe_3O_4-MWCNTs powder (**b**) and mortar specimens (**c**).

2.3. Mixture Proportions and Testing

In this study, a total of four mixes containing 0, 1, 2, and 3 wt% Fe_3O_4-MWCNTs nanocomposite (MAC) with a constant water-to-cement ratio of 0.5 were produced. Table 2 presents the mixing proportions adopted in this study. The rationale behind the mixing proportions was the authors' experience and the trials conducted. The curing regime adopted in this study was ambient curing with a constant temperature and humidity of 23 ± 2 °C and >95%, respectively.

Table 2. Mixing proportions adopted in this study.

Specimen	Sand (g)	Cement (g)	MAC (g)	MAC (Binder wt %)	Water (g)
Reference	1350.0	450	0	0	225
MAC1	1345.5	450	4.5	1	225
MAC2	1341.0	450	9.0	2	225
MAC3	1336.5	450	13.5	3	225

To evaluate the physico-mechanical properties of the produced cementitious composites, a series of tests, including apparent porosity, water absorption, unit weight (based on ASTM C642 [36]), and compressive strength (based on ASTM C349 [37]), were conducted. The electrical resistivity of the mortar samples was determined according to the two-point uniaxial Wenner probe and ASTM C1760-12 [38]. In this regard, the resistance measurement was carried out with a two-point uniaxial method, which is a general measurement method whereby the resistance (R) value is obtained by applying a certain tension between two parallel surfaces of the mortar sample, and the resistivity (ρ) value is calculated from Equation (3).

$$R = \frac{\rho L}{A}\ (\Omega) \tag{3}$$

Additionally, ultrasonic pulse velocity (UPV), SEM and EDS tests were conducted on different mixes to evaluate their microstructural development.

3. Results and Discussion

3.1. Characterization of Synthesised MWCNTs and Fe_3O_4-MWCNTs

3.1.1. X-ray Diffractometer (XRD)

Figure 3 presents the XRD patterns of the synthesized MWCNTs and Fe_3O_4-MWCNTs. The distinct peaks at 2θ of about 26.06° and 43.93° in Figure 3a are attributed to (002) and (100) planes of the MWCNTs, respectively, as also noted by Ref. [39]. The peaks at 2θ of 26.27° (220), 30.72° (220), 35.66° (311), 43.49° (400), 57.41° (511) and 63.09° (440) in Figure 3b correspond to magnetite (Fe_3O_4) phase [39], and indicate that Fe_3O_4 particles have a cubic spinal structure [40,41]. These data reveal that the Fe_3O_4-MWCNT particles were synthesized successfully.

3.1.2. FTIR Spectroscopy

Figure 4 presents the FTIR spectra of MWCNTs and Fe_3O_4-MWCNTs. Based on Figure 4, the presence of functional groups within MWCNTs and Fe_3O_4-MWCNTs can be observed which are very similar. For both materials, the peaks at 3738 cm^{-1} and 3871 cm^{-1} belong to -OH groups of alcohols and phenols [42]. Further, the peaks at 2350 cm^{-1} and 2110 cm^{-1} represent C-C and C-C-H stretching, respectively. The peak at 1990 cm^{-1} belongs to the C-C stretch, while 1539 cm^{-1} and 1560 cm^{-1} peaks are due to stretching vibrations of carbonyl (C=O) and ethylene (-C=C-) in the aromatic ring, respectively. Tolba et al. [42] reported a similar sharp band for Fe_3O_4-impregnated MWCNTs. Further, the peak at 1446 cm^{-1} represents the C-H deformation vibration. C-OH stretching vibration was observed at a wavelength of 1047 cm^{-1}.

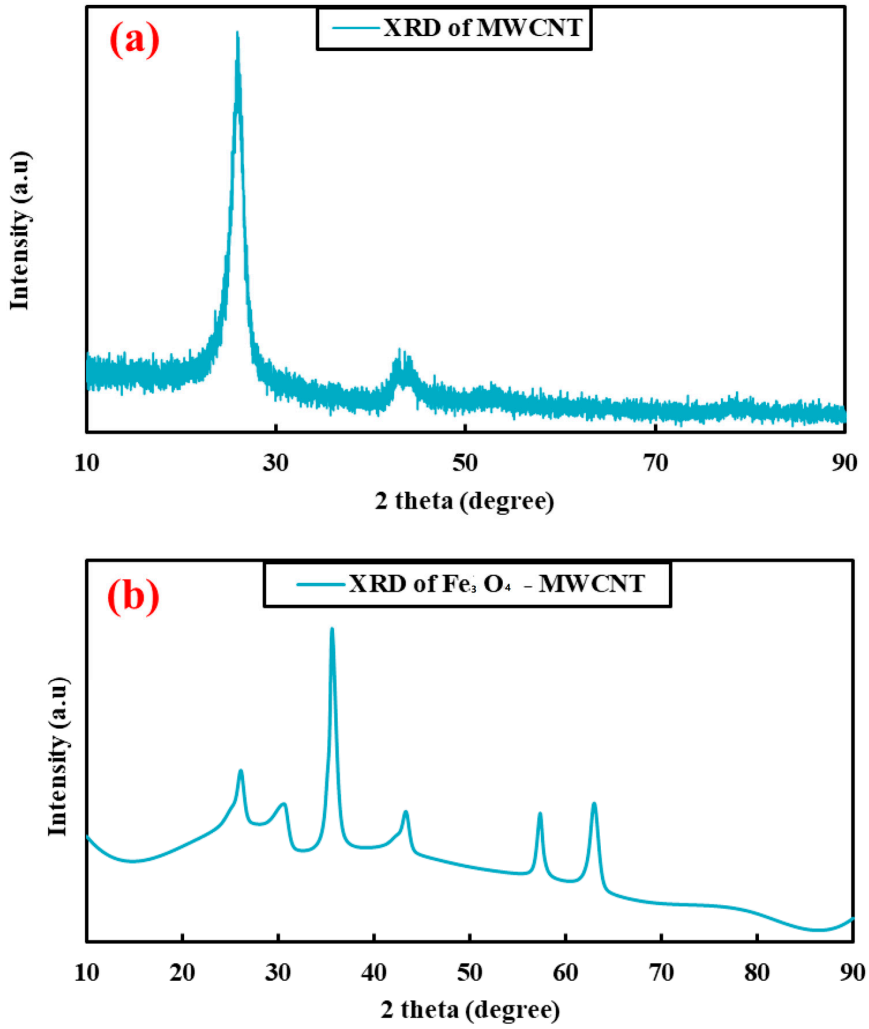

Figure 3. XRD patterns of MWCNT (**a**) and Fe_3O_4-MWCNT (**b**).

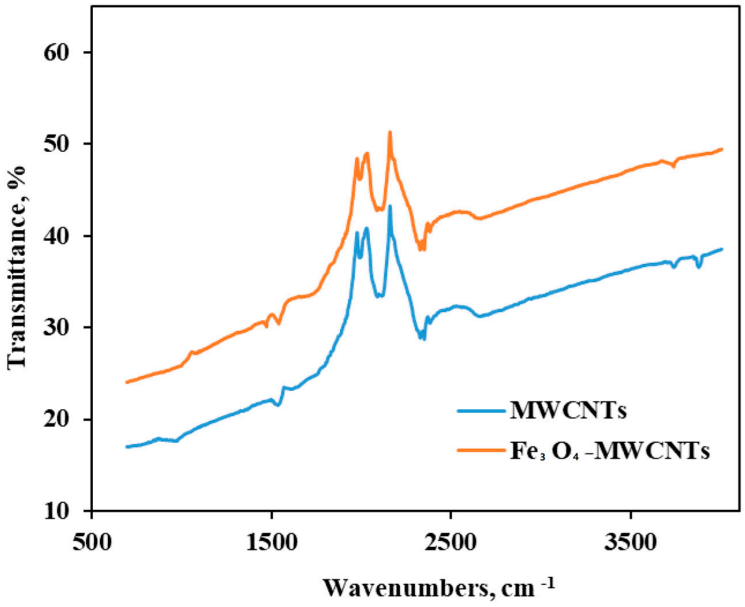

Figure 4. FTIR spectra of MWCNTs and Fe_3O_4-MWCNTs.

3.1.3. TEM

TEM images of MWCNTs and Fe_3O_4-MWCNTs are shown in Figure 5. Based on Figure 5a, the MWCNTs had a curved shape and they were not considerably agglomerated, which potentially refers to their high surface area to be incorporated in cementitious composites, as noted by Ref. [42]. According to Figure 5b, in Fe_3O_4-impregnated MWCNTs, MWCNTs were captured with Fe_3O_4 particles with a generally higher agglomeration than that in MWCNTs. This can be due to the high attraction of magnatized nano Fe_3O_4 that is stronger than the repulsive Van der Waals forces between the MWCNTs [39,42].

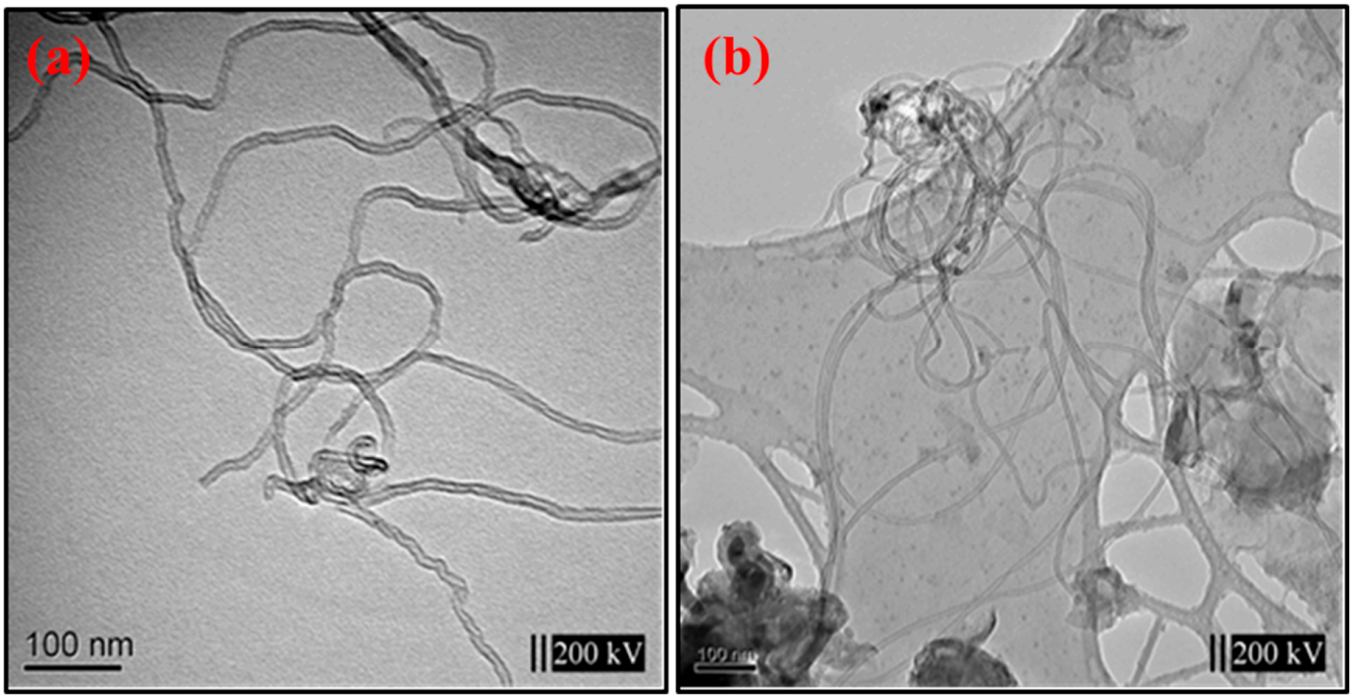

Figure 5. TEM of MWCNTs (**a**) and Fe_3O_4-MWCNTs (**b**).

3.1.4. SEM/EDS

Figure 6a–c presents SEM images of MWCNTs. Based on these figures, a relatively imhonogenous distribution of MWCNTs can be seen that makes the dispersion of these materials a relatively challenging process, as also discussed by Ref. [43]. Figure 6d shows SEM image of Fe_3O_4-impregnated MWCNTs. Based on this figure, the Fe_3O_4 particles were dispersed throughout the MWCNTs. Further, Figure 6e shows the SEM image of grown MWCNTs with their respective size ranging from ~30 to 48 nm.

The results of EDS and elemental mapping images of Fe_3O_4-MWCNTs are presented in Figure 7. Based on these figures, the highest element present in Fe_3O_4-impregnated MWCNTs was carbon, followed by iron and a slight content of embedded oxygen.

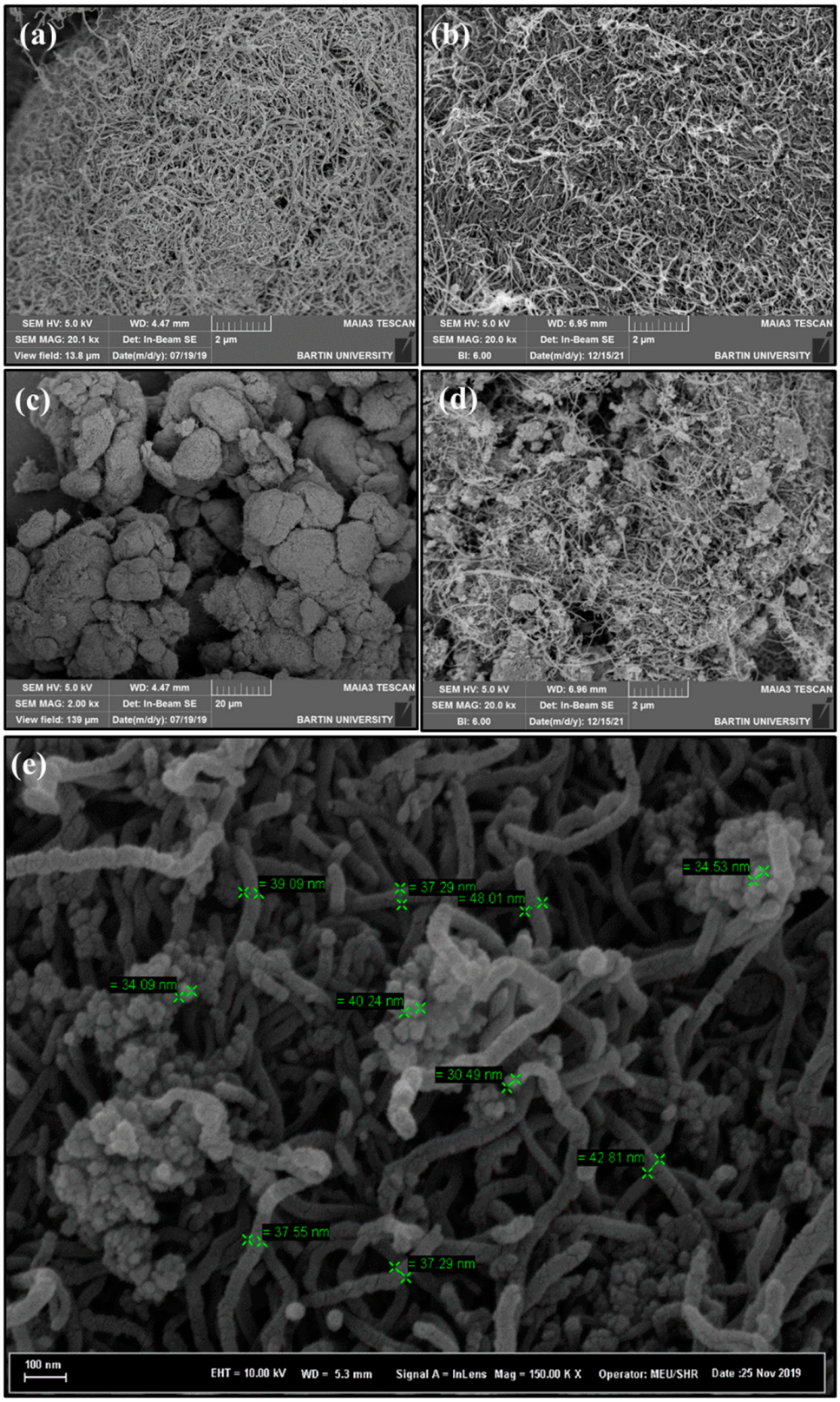

Figure 6. SEM images of MWCNTs (**a**–**c**), Fe_3O_4-MWCNTs (**d**,**e**).

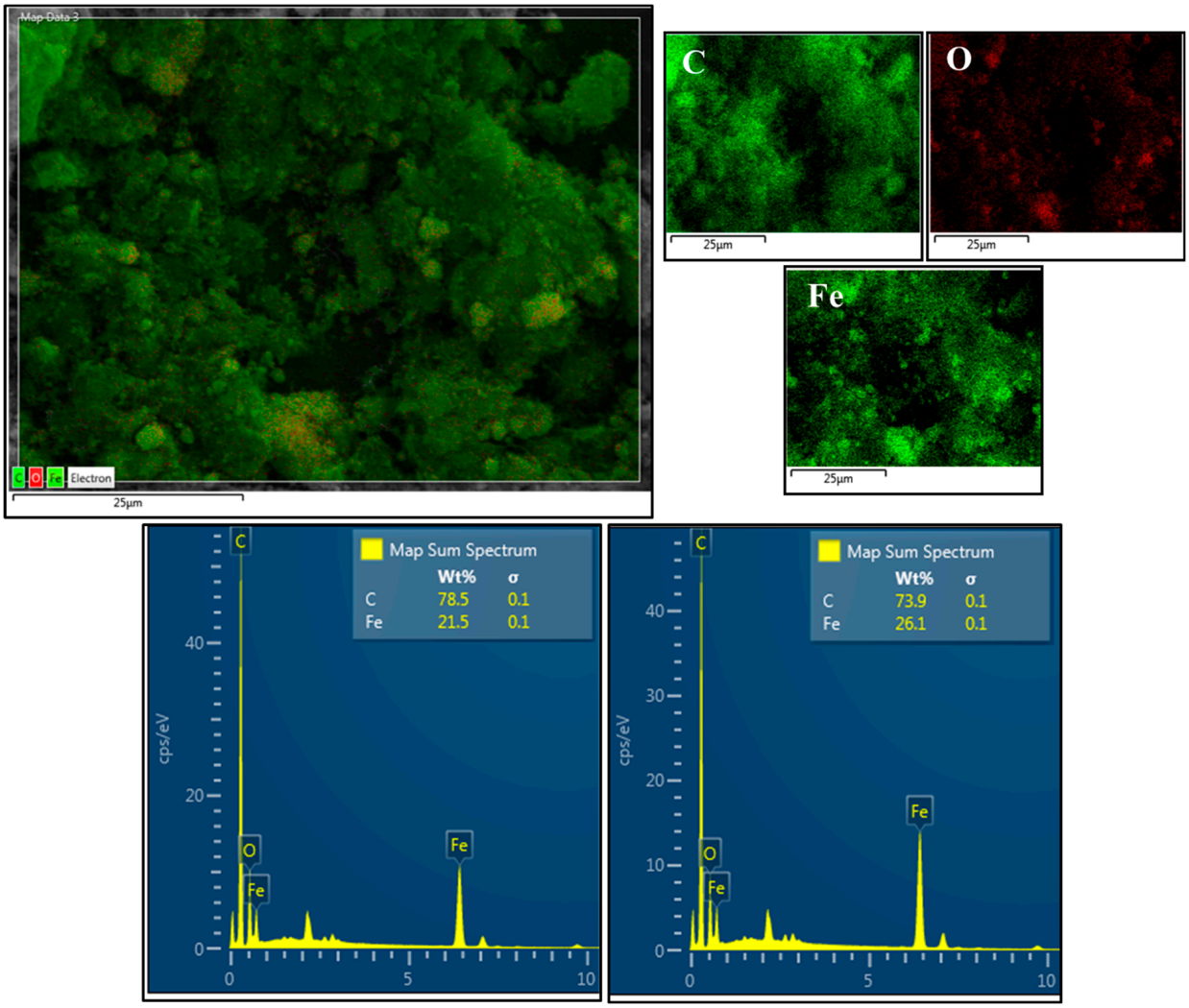

Figure 7. Elemental mapping images of Fe_3O_4-MWCNT and EDS analysis of Fe_3O_4-impregnated MWCNTs.

3.2. Characterization of Mortars

3.2.1. Unit Weight

Figure 8 shows the unit weight of various mixes measured after 28 days of curing. Based on the figure, it can be seen that the inclusion of Fe_3O_4-impregnated MWCNT reduced the unit weight of mixes. Mixes containing 1, 2, and 3% Fe_3O_4-impregnated MWCNTs experienced 2.4, 4.3, and 10.6% lower unit weight than the reference mix with 0% Fe_3O_4-MWCNTs nanocomposite, respectively. The decrease in the unit weight with an increased Fe_3O_4-MWCNTs nanocomposite content can be due to the increased content of air cavities in the mixes, as will be noted in Section 3.2.6. Florez et al. [44] reported that the inclusion of Fe_3O_4 up to 5% slightly increased (~5%) the density of cement composites; however, further increase in Fe_3O_4 up to 50% led to a 22% reduction in the density of composite. Based on the mentioned performance of the Fe_3O_4 and MWCNTs, the reduction in the unit weight in MAC1, 2 and 3 can be due to the combined effect of Fe_3O_4 and MWCNTs [45] that can potentially allow air bubbles to remain within the mixture microstructure where the Fe_3O_4-MWCNTs particles are not well dispersed. Similar results are reported in Ref. [45].

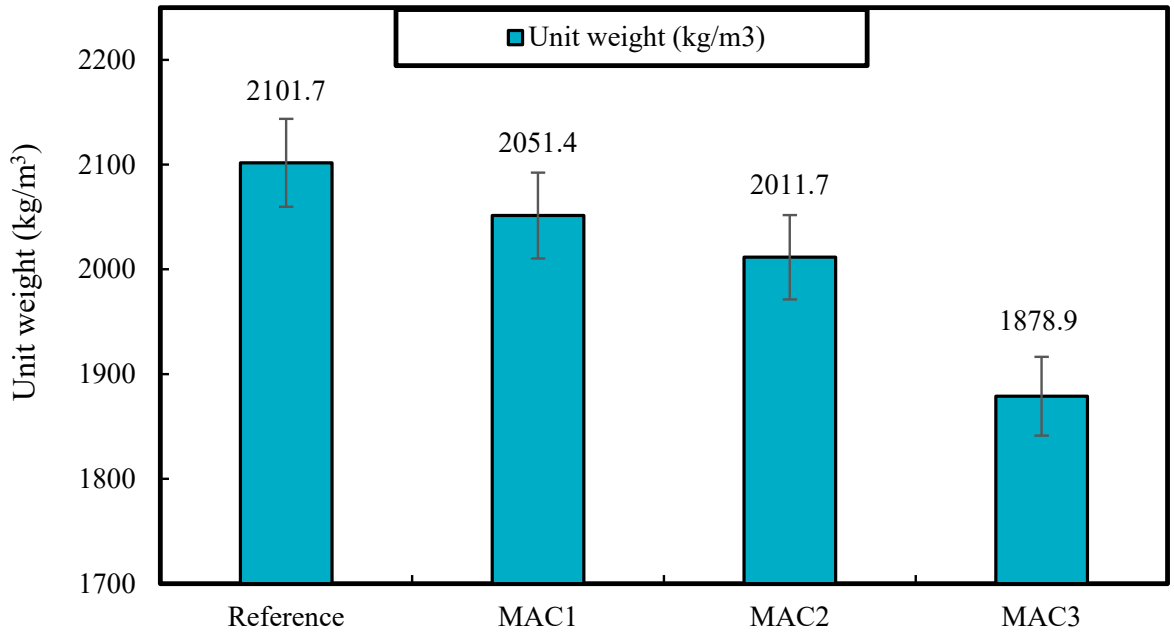

Figure 8. Unit weight of different mixes.

3.2.2. Compressive Strength

Figure 9a shows the results of 7 and 28 days of compressive strength of different mixes. Based on the figure, the highest and lowest compressive strength values on 28th day were 34.8 MPa for the reference mix and 17.4 MPa for the MAC3 mix, respectively. As can also be seen in the figure, the inclusion of 1, 2, and 3% Fe_3O_4-MWCNTs nanocomposite reduced the 7-day compressive strength values by ~47, 42 and 60%, respectively. This result is in harmony with those discussed in Sections 3.2.2–3.2.4 and points to the reduced physical-mechanical properties of the produced mortars when Fe_3O_4-MWCNTs are added to the mixture. Similarly, on the 28th day, the inclusion of Fe_3O_4-MWCNTs nanocomposite reduced the compressive strength values by ~35, 43, and 50%, respectively. According to Jiao et al. [46], the inclusion of conductive particles has the potential to destroy the early C-S-H links between cement particles and can result in the agglomeration of mixture materials and a loss of mechanical properties. This agglomeration can not only cause an increase in the content of air cavities, but also an increase in the capillary water content, which results in a reduction of the mix strength [45]. This effect can further be confirmed through the opposite results documented by previous studies that used Fe_3O_4 and MWCNTs individually and reported a reduction of microstructural porosity. For instance, Cwirzen et al. [47] reported up to 50% increase in compressive strength of specimens produced with only 0.045% MWCNTs and associated this with the chemical bonds between the OH and the C-S-H phase of the cement matrix which helps the imposed stress to transfer. Similar results have also been documented by Ref. [48] which utilized 0.2 wt% MWCNTs and Ref. [44] which used up to 12.5% Fe_3O_4 and reported an increase of up to 50% in compressive strength values. However, the opposite impact of the Fe_3O_4-MWCNTs addition can be due to the combined effect of the two nano materials that considerably reduces the dispersion rate of materials within the mixture. Also, from the figure, it can be seen that the compressive strength of MAC2 is higher than MAC1 for 7 days but not 28 days. The reason for this is believed to be the statistical error and variation in the results.

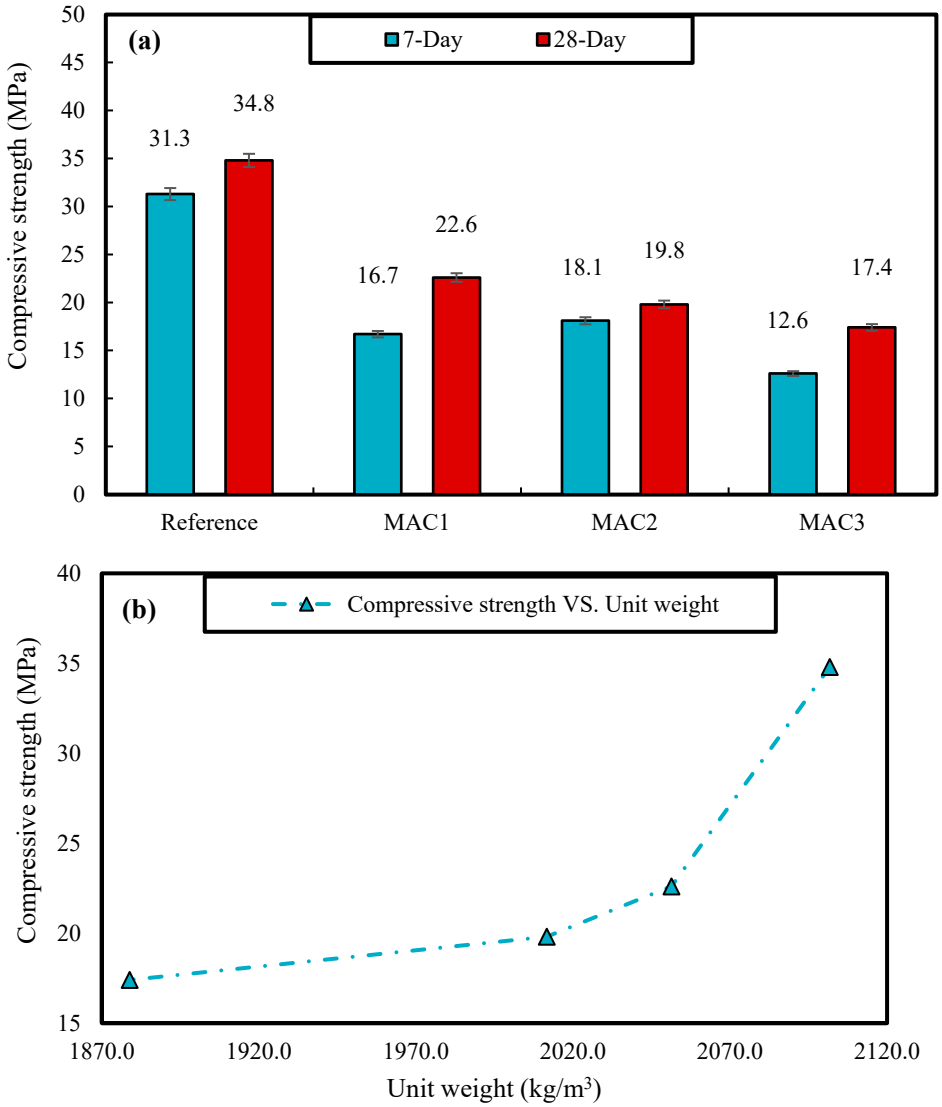

Figure 9. 7th and 28th-day compressive strength (**a**) and the relationship between 28-day compressive strength and unit weight of different mixes (**b**).

Figure 9b shows the variation of 28-day compressive strength with the unit weight of different mixes. Based on the figure, the compressive strength values enhanced non-linearly when the unit weight increased. This non-linearity can be indicative of the effect of the magnetic force on the mixture's particle dispersion. A denser content of materials in the mixture causes less material agglomeration and air cavities [45].

3.2.3. Apparent Porosity

Figure 10 shows the results of the apparent porosity test conducted on different mixes after 28 days of curing. Based on the figure, it can be seen that the highest and lowest apparent porosity values were 26.8% for the reference mix and 15.3% for MAC3 mix, respectively. It is also shown that the inclusion of 1, 2, and 3% Fe_3O_4-MWCNTs nanocomposite increased the porosity of the mixes by ~30, 42, and 75%, respectively. Based on the results, the increase in the porosity can be mainly due to the creation of small initial strains in the microstructure of the mixes that are potentially caused by Fe_3O_4-MWCNTs nanocomposite, which results in a higher elastic yield stress than the materials limit, causing micro-agitation and an increase of micropores [46,49]. By comparing Figures 9a and 10, an increased porosity of the mixture caused a decrease in the compressive strength, which

indicates that the results of porosity were aligned with those of compressive strength values reported in Section 3.2.2. This correlation is shown in Figure 9b.

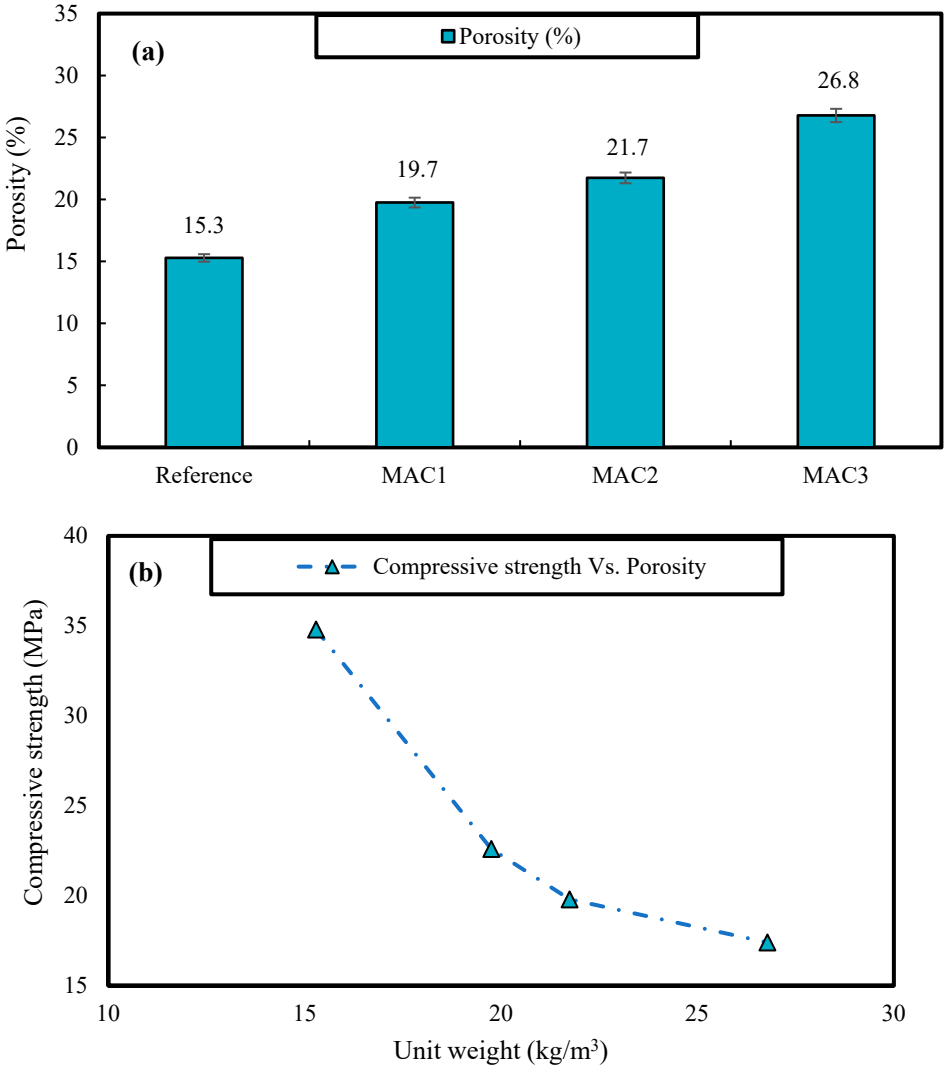

Figure 10. The porosity of different mixes (**a**) and the correlation between the compressive strengths vs. porosity (**b**).

3.2.4. Water Absorption

The 28th-day water absorption of different mixes is presented in Figure 11a. Based on the figure, it can be observed that the inclusion of Fe_3O_4-MWCNTs nanocomposite consistently increased the water absorption values, from 7.3% in the reference mix to 14.3% in the MAC3 mix. The reason for this increased absorption can be an increased porosity of the mixes with an increased Fe_3O_4-MWCNTs nanocomposite content, as was discussed in Section 3.2.3. This relationship between water absorption and porosity can be further seen in Figure 11b, which shows a linear increase trend between water absorption and porosity with an increase in Fe_3O_4-MWCNTs nanocomposite content. According to Ref. [50], the inclusion of MWCNTs can slightly reduce the capillary porosity of cementitious composites through channeling and partially filling micro pores. Nonetheless, an opposite result was found in this study, which can be due to the effect of Fe_3O_4-MWCNTs nanocomposite and improper dispersion of mixture materials [46,49].

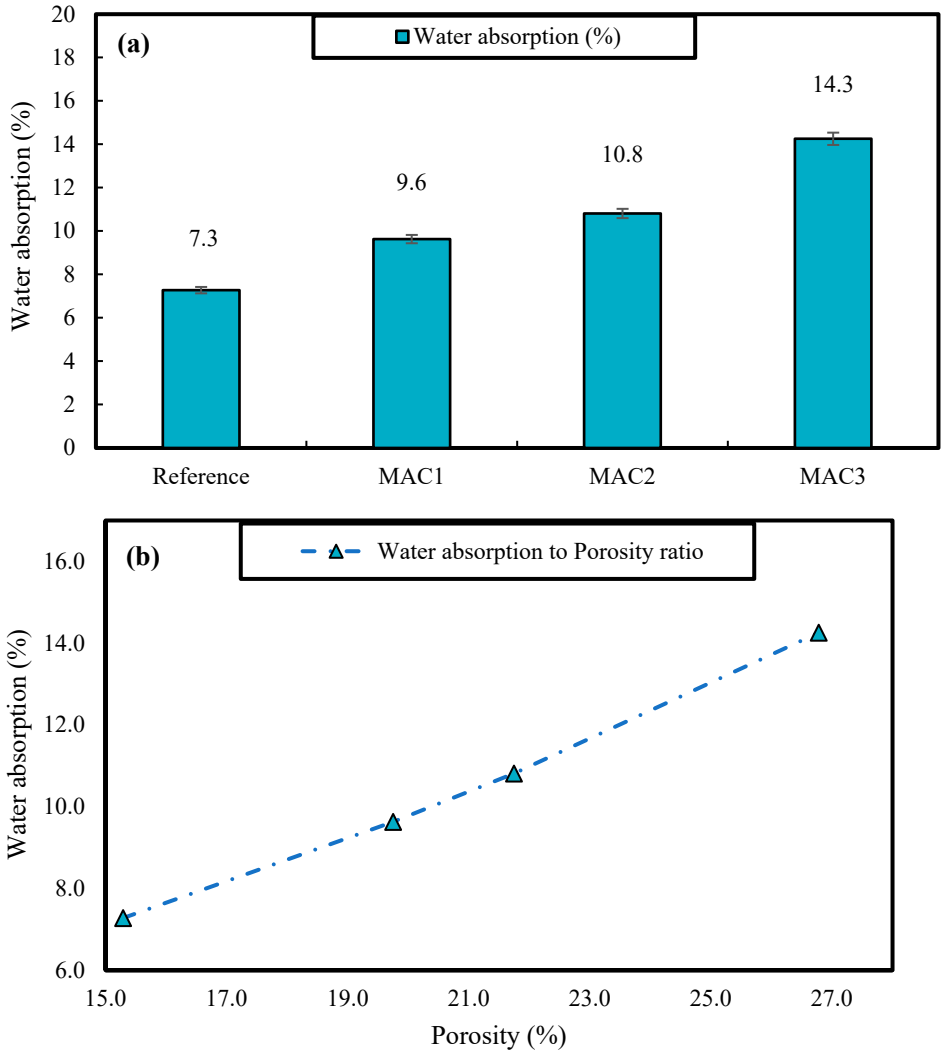

Figure 11. Water absorption (**a**) and the relationship between water absorption and porosity of different mixes (**b**).

3.2.5. Sorptivity

The result of sorptivity test on different mixes is presented in Figure 12. Based on the figure, the initial sorptivity rate was rather similar in all mixes both in depth and the slope of increase, presented in the figure. However, after ~24 $sec^{0.5}$, MAC mixes exhibited a steeper water penetration rate compared to the reference mix which can be due to water passing the initial surface layer. In that respect, at 294 $sec^{0.5}$, MAC2 had ~7.7 mm penetration depth, which was higher than MAC3 with ~7.2 mm penetration depth, and ~97% higher than the reference mix with ~3.9 mm penetration depth. The reason for a higher sorptivity of mixes containing Fe_3O_4-MWCNTs nanocomposite than that of the reference mix is the higher porosity of the mixes containing Fe_3O_4-MWCNTs nanocomposite resulted from the early effect of the magnetic field, especially around the surface of nano MWCNTs and Fe_3O_4. This has also been discussed by Jiao et al. [46] that reported nano Fe_3O_4 particles can move from magnetic clusters when the magnetic field is applied and results in significant variation of the hardened cementitious paste. This can be further confirmed by the opposite results obtained by other studies that utilized nano Fe_3O_4 [51] and MWCNTs [45] separately and reported a reduction of porosity and permeability.

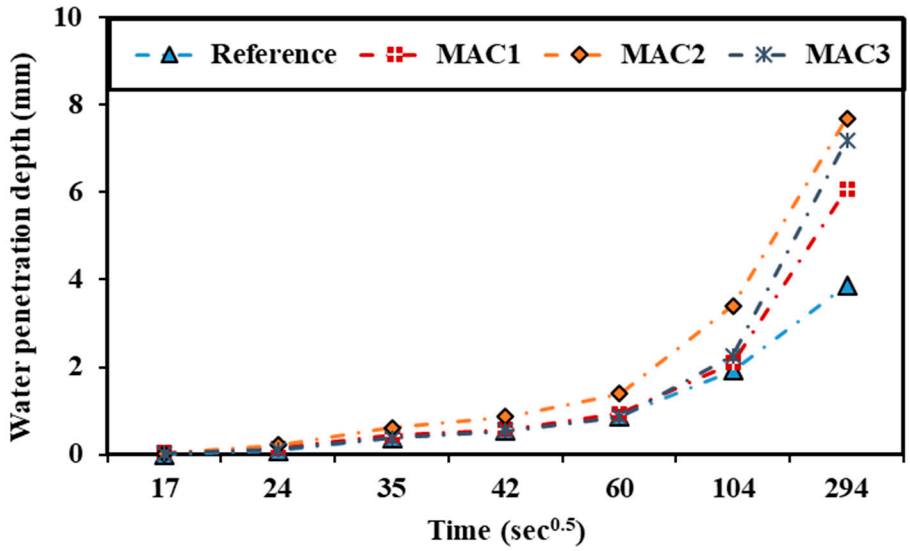

Figure 12. Sorptivity of different mixes.

3.2.6. Electrical Resistivity

The result of the electrical resistivity of mixes is presented in Figure 13. Based on this figure, as the content of Fe_3O_4-MWCNTs nanocomposite is increased the resistivity values have constantly lowered. For instance, at 0% Fe_3O_4-MWCNTs nanocomposite content, the mean value of electrical resistivity is found to be ~199 Ω·m. At 1, 2 and 3% Fe_3O_4-MWCNTs nanocomposite, however, these values changes to ~139, 90 and 64 Ω·m. According to Refs. [52,53] in ferromagnetic materials, electrical resistance is the result of the scattering of conduction electrons with the unfilled inner shell electrons that overlap. This, in other words, refers to the effect of conductivity in lowering the electrical resistivity of the produced specimens [54]. A similar reduction of resistivity values can be seen when the voltage is increased. As discussed by Ref. [54], voltage is inversely related to the resistance values, which can be the reason for slightly lower resistance as the applied voltage is increased. Table 3 shows the comparison of the study with the literature in terms of electrical resistivities.

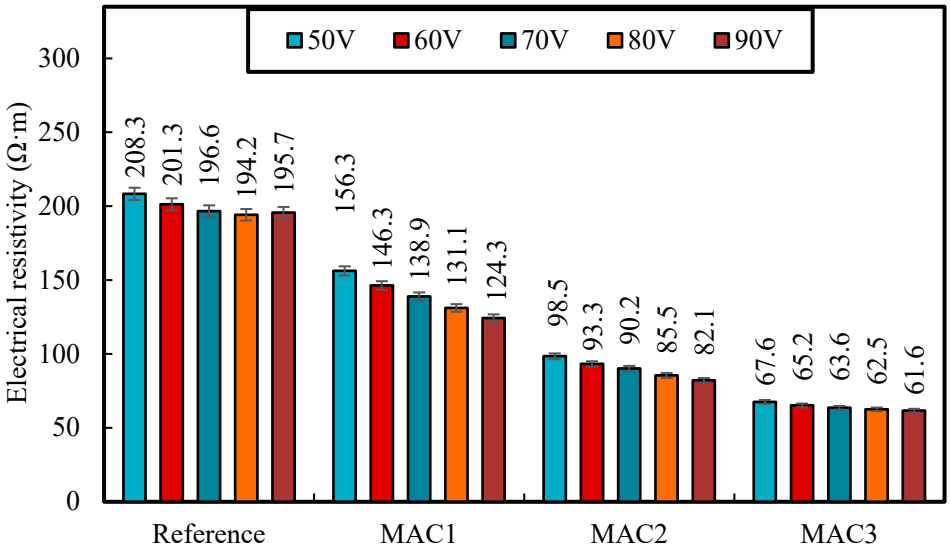

Figure 13. Electrical resistivity of various mixes under different voltage.

Table 3. Comparison with the literature in terms of electrical resistivities.

Matrix	Additive	Electrical Resistivity (Ω·m)	Reference
Mortar	Graphite	75	[55]
Mortar	Graphene	2500	[56]
Cement	Carbon fibre	6.75	[57]
Cement	Steel fiber	0.57	[58]
Cement	Blast-furnace slag	596.7	[59]
Cement	Pristine carbon fiber	35	[60]
Cement	Carbon fiber treated with piranha solution	5	[60]
Cement	Fe_3O_4-MWCNTs nanocomposite	61.6	This study

3.2.7. UPV

The result of the UPV test is presented in Figure 14a. Based on this figure, the inclusion of Fe_3O_4-MWCNTs nanocomposite has relatively reduced the UPV speed values. As can be seen in the figure, at 1, 2 and 3% Fe_3O_4-MWCNTs nanocomposite content, mixes presented ~6, 12 and 18% reduction in the UPV values. This, in part, can be the result of the higher porosity of the MAC mixes, as discussed in Section 3.2.3. Another reason for this can potentially be due to the adverse effect of conductive energy interfering with the passing UPV [52,53]. A general classification of UPV results can also be found at Refs. [61,62]. Further, Figure 14b presents the relationship between the compressive strength versus UPV results which further verifies the values achieved in this study.

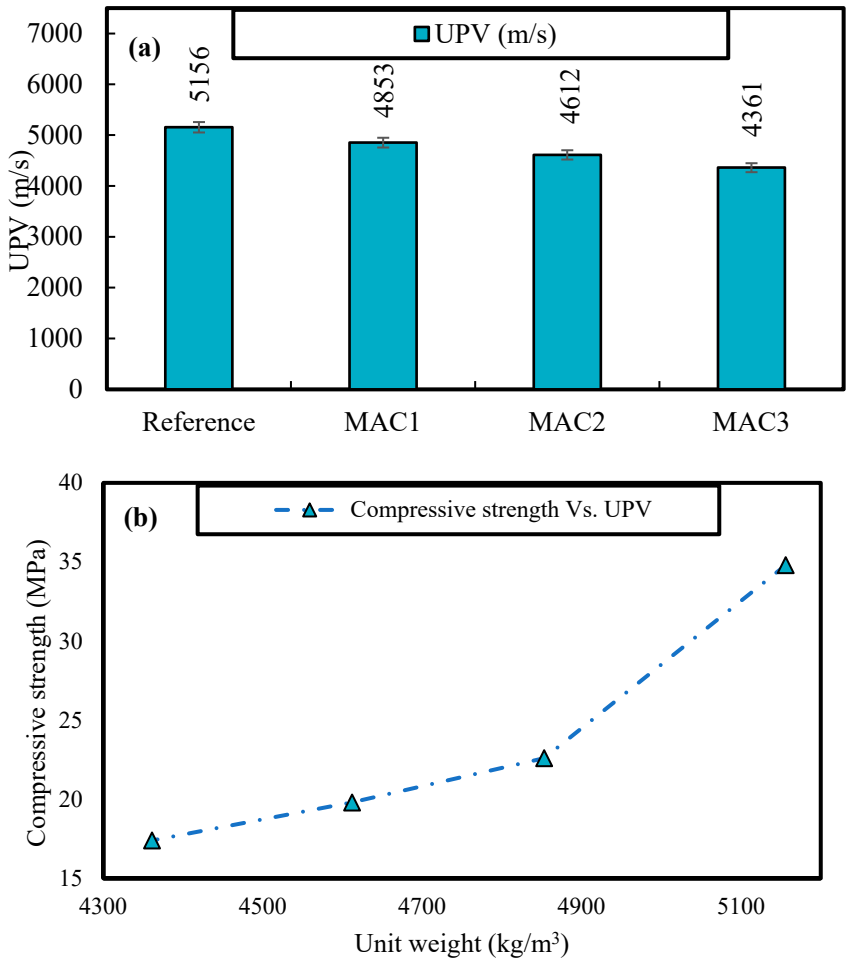

Figure 14. UPV result of various mixes (**a**) and the correlation between compressive strength versus that of UPV (**b**).

3.2.8. SEM/EDS of Mortars

Figure 15 presents the SEM images taken from the reference mix versus MAC3. Based on Figure 15a,b, the reference mix had comparatively a higher number of cracks with larger widths than MAC3. The lower width of cracks in MAC3 than that of the reference mix can be due to the inclusion of 3% MWCNTs that bridges micro and nano-sized cracks [63]. Further, Figure 15c,d shows that a larger number of air voids and cavities were dispersed throughout the MAC3 when compared to the reference mix which can explain why higher porosity and water absorption values are achieved for MAC3 in Sections 3.2.3 and 3.2.4. Nonetheless, this can be due to the initial strain of mixes with Fe_3O_4-impregnated MWCNTs that can lead to the creation of localized voids in the microstructure of the mix [46] resulting in lower strength values, as reported in Section 3.2. From Figure 15e,f, it can be seen that the MAC3 mix contained MWCNTs filling the voids and channeling hydration products. In turn, from Figure 15g,h it can be seen that the formation and origin of cracks in MAC3 is somewhat different when compared to that of the reference mix. Such differences in porosity can possibly result in anisotropic behavior and varying performance. This can further be seen in Figure 15i,j, which shows that the calcium-silicate-hydrate (C-S-H) products in MAC3 were more dispersed and inhomogeneous compared to those of the reference mix which can explain why lower compressive strength values are achieved (Section 3.2.2) in MAC3. Therefore, the cracks in MAC3 (shown in Figure 15h) mostly originated from the air-void cavities while the cracks in the reference mix (shown in Figure 15h) were more of shrinkage style ones. Although the inclusion of MWCNTs could reduce the width of cracks in MAC3, it could not completely reduce the effect of air cavities. This is further confirmed in Section 3.2.3. that MAC3 specimens are found to have higher apparent porosity values.

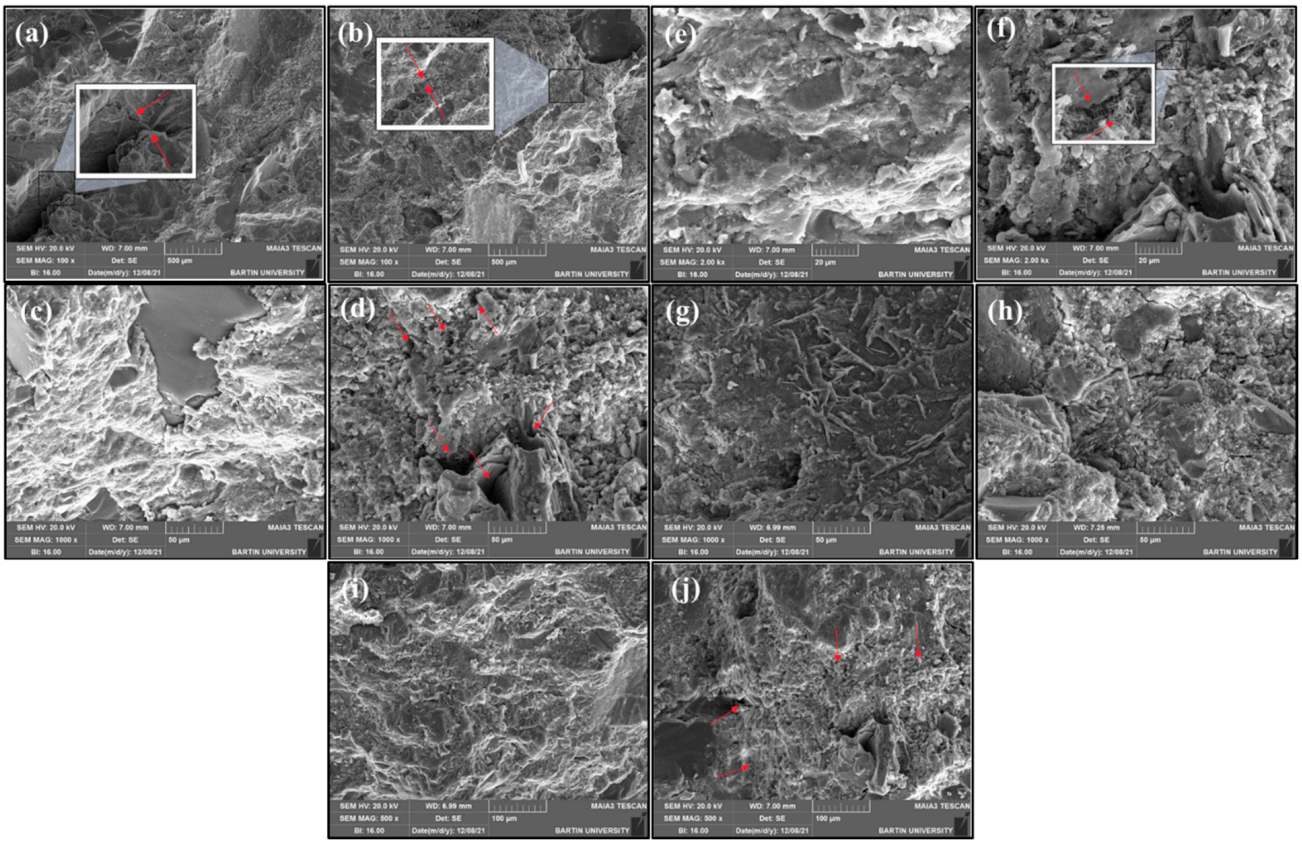

Figure 15. SEM images of reference (**a**,**c**,**e**,**g**,**i**) versus MAC3 (**b**,**d**,**f**,**h**,**j**) mortar mixes.

Table 4 presents the result of the EDS (weight %) of each mix. Based on the table, it can be seen that when the content of Fe_3O_4-MWCNTs nanocomposite in a mix increased, the weight % of Ca and Fe elements increased. In that respect, MAC3 exhibited 15% higher

Ca and 7.6% higher Fe content than the reference mix. Further from Table 3, it can be seen that when the content of Fe_3O_4-MWCNTs nanocomposite increased, the mean Si content decreased (up to 2.3%).

Table 4. EDS (weight %) of Reference, MAC1, MAC2, and MAC3 mixes.

Mix	Ca	Si	Na	Al	K	Fe
Reference	63.28	24.61	3.70	5.45	6.46	4.17
MAC1	63.85	21.96	5.90	8.57	6.20	3.63
MAC2	68.28	16.64	0	5.41	10.4	6.30
MAC3	72.78	19.01	3.40	3.26	3.20	7.35

4. Conclusions

In this study, Fe_3O_4-MWCNTs nanocomposites were synthesized using a chemical vapor deposition (CVD) unit of iron oxide (Fe_3O_4) and multi-walled carbon nanotubes (MWCNTs). Further, Fe_3O_4-MWCNTs nanocomposite (MAC) were added to mortar mixes at 1, 2 and 3 wt% to investigate their mechanical, electrical conductivity and durability properties. The results of this study can be summarized as follows:

- Based on SEM analysis, larger air-void cavities were embedded in the mortars containing Fe_3O_4-MWCNTs nanocomposite than that of the unreinforced mortar, which can potentially be due to the adverse early effect of conductive energy/force that creates slight strains in fresh mixtures, developing localized air cavities in the mortar microstructure. Also, it is a possibility that the combined effect of two nano materials (e.g., in this case, Fe_3O_4 and MWCNTs) is responsible for the coagulation of materials that can reduce the mixing efficiency and result in lower physical-mechanical properties.
- The origin of cracks in mortars containing Fe_3O_4-MWCNTs nanocomposite was different from that of unreinforced mortars and is potentially caused by the air cavities. This observation was further confirmed by the inhomogenously dispersed C-S-H in the microstructure of the mortars containing a higher content of Fe_3O_4-MWCNTs nanocomposites. This can cause anisotropic behavior of the produced mortars which, under stress can have variable performance.
- Mortars containing 3% Fe_3O_4-MWCNTs nanocomposite exhibited ~11, 75, 95, 46, and 50% lower unit weight, apparent porosity, water absorption, sorptivity, and compressive strength at 28 days of curing than unreinforced mortar, respectively. The reason behind that can be the effect of Fe_3O_4-MWCNTs being exerted on the freshly mixed materials that can cause a series of localized flocculation and air cavities within the mixture. This hypothesis is aligned with the observations on SEM micrographs that showed an inhomogeneous microstructure of the mortars produced with Fe_3O_4-MWCNTs.

The results of this study point to the successful use of Fe_3O_4-MWCNTs nanocomposite to improve the electrical conductivity properties of cementitious materials, indicating their great potential for smart and self-sensing concrete applications. Nonetheless, future studies in this area can potentially provide further details on the topic of how best to avoid its adverse effect on the initial microstructural formation of cementitious composites. Additionally, the capacity of various cementitious composites in storing magnetic energy can be another topic for further evaluation. In either case, the results point to the importance of magnetic force that engineers can further evaluate and take advantage of in the production of smart or engineered materials.

Author Contributions: Conceptualization, V.S., O.G. (Omer Guler), A.S., A.Y., O.G. (Osman Gencel), and T.O.; methodology V.S., O.G. (Omer Guler), A.S., A.Y., O.G. (Osman Gencel) and T.O.; validation, V.S., O.G. (Omer Guler), M.N., A.S., A.Y., O.G. (Osman Gencel), A.G., and T.O.; formal analysis, V.S., O.G. (Omer Guler), A.S., A.Y., O.G. (Osman Gencel) and T.O. investigation, V.S., O.G. (Omer Guler), A.S., A.Y., O.G. (Osman Gencel) and T.O.; resources, V.S., O.G. (Omer Guler), A.S., A.Y., O.G. (Osman Gencel) and T.O.; data curation, V.S., O.G. (Omer Guler), A.S., A.Y., O.G. (Osman Gencel) and T.O.; writing—original draft preparation, M.N.; writing—review and editing, M.N., A.G., O.G. (Osman Gencel), T.O.; visualization, M.N., A.G., O.G. (Osman Gencel), T.O.; supervision, V.S., O.G. (Omer Guler), A.S., A.Y., O.G. (Osman Gencel) and T.O.; project administration, V.S., O.G. (Omer Guler), A.S., A.Y., O.G. (Osman Gencel) and T.O.; funding acquisition, V.S., O.G. (Omer Guler), A.S., A.Y., O.G. (Osman Gencel) and T.O. All authors have read and agreed to the published version of the manuscript.

Funding: No funding was received for this study.

Institutional Review Board Statement: Not applicable.

Informed Consent Statement: Not applicable.

Data Availability Statement: Not applicable.

Conflicts of Interest: The authors declare no conflict of interest.

References

1. Gencel, O.; Nodehi, M.; Hekimoğlu, G.; Ustaoğlu, A.; Sarı, A.; Kaplan, G.; Bayraktar, O.Y.; Sutcu, M.; Ozbakkaloglu, T. Foam Concrete Produced with Recycled Concrete Powder and Phase Change Materials. *Sustainability* **2022**, *14*, 7458. [CrossRef]
2. Wei, J.; Zhao, L.; Zhang, Q.; Nie, Z.; Hao, L. Enhanced thermoelectric properties of cement-based composites with expanded graphite for climate adaptation and large-scale energy harvesting. *Energy Build.* **2018**, *159*, 66–74. [CrossRef]
3. Ibarra-Sierra, V.G.; Sandoval-Santana, J.C.; Kunold, A.; Herrera, S.A.; Naumis, G.G. Dirac materials under linear polarized light: Quantum wave function time evolution and topological Berry phases as classical charged particles trajectories under electromagnetic fields. *J. Phys. Mater.* **2022**, *5*, 014002. [CrossRef]
4. Lewis, L.H.; Jiménez-Villacorta, F. Perspectives on Permanent Magnetic Materials for Energy Conversion and Power Generation. *Metall. Mater. Trans. A* **2013**, *44*, 2–20. [CrossRef]
5. Dent, P.C. Rare earth elements and permanent magnets (invited). *J. Appl. Phys.* **2012**, *111*, 07A721. [CrossRef]
6. Jiao, D.; Lesage, K.; Yardimci, M.Y.; El Cheikh, K.; Shi, C.; De Schutter, G. Structural evolution of cement paste with nano-Fe3O4 under magnetic field—Effect of concentration and particle size of nano-Fe_3O_4. *Cem. Concr. Compos.* **2021**, *120*, 104036. [CrossRef]
7. Tjong, S.C. *Carbon Nanotube Reinforced Composites*; Wiley: Hoboken, NJ, USA, 2009. [CrossRef]
8. Javey, A.; Kong, J. *Carbon Nanotube Electronics*; Springer: Boston, MA, USA, 2009. [CrossRef]
9. Madenci, E.; Özkılıç, Y.O.; Aksoylu, C.; Asyraf, M.R.M.; Syamsir, A.; Supian, A.B.M.; Mamaev, N. Buckling Analysis of CNT-Reinforced Polymer Composite Beam Using Experimental and Analytical Methods. *Materials* **2023**, *16*, 614. [CrossRef]
10. Madenci, E.; Özkılıç, Y.O.; Aksoylu, C.; Asyraf, M.R.M.; Syamsir, A.; Supian, A.B.M.; Elizaveta, B. Experimental and Analytical Investigation of Flexural Behavior of Carbon Nanotube Reinforced Textile Based Composites. *Materials* **2023**, *16*, 2222. [CrossRef]
11. Onuralp, Y.; Madenci, E.; Yasin, Ö.; Özkılıç, O.; Hakamy, A.; Hakamy, A.; Tounsi, A. Experimental tensile test and micro mechanic investigation on carbon nanotube reinforced carbon fiber composite beams. *Adv. Nano Res.* **2023**, *14*.
12. Harris, P.J.F. *Carbon Nanotube Science*; Cambridge University Press: Cambridge, UK, 2009. [CrossRef]
13. Samadishadlou, M.; Farshbaf, M.; Annabi, N.; Kavetskyy, T.; Khalilov, R.; Saghfi, S.; Akbarzadeh, A.; Mousavi, S. Magnetic carbon nanotubes: Preparation, physical properties, and applications in biomedicine. *Artif. Cells Nanomed. Biotechnol.* **2018**, *46*, 1314–1330. [CrossRef]
14. Pantano, A. *Carbon Nanotube Based Composites: Processing, Properties, Modelling and Application*; Smithers Rapra Technology: Shropshire, UK, 2012.
15. Nayfeh, M.H. *Fundamentals and Applications of Nano Silicon in Plasmonics and Fullerines*; Elsevier: Amsterdam, The Netherlands, 2008; pp. 287–309. [CrossRef]
16. Ong, Y.T.; Ahmad, A.L.; Zein, S.H.S.; Tan, S.H. A review on carbon nanotubes in an environmental protection and green engineering perspective. *Braz. J. Chem. Eng.* **2010**, *27*, 227–242. [CrossRef]
17. Centi, G.; Perathoner, S. Carbon Nanotubes for Sustainable Energy Applications. *ChemSusChem* **2011**, *4*, 913–925. [CrossRef]
18. Mohammed, I.A.; Bankole, M.T.; Abdulkareem, A.S.; Ochigbo, S.S.; Afolabi, A.S.; Abubakre, O.K. Full factorial design approach to carbon nanotubes synthesis by CVD method in argon environment. *S. Afr. J. Chem. Eng.* **2017**, *24*, 17–42. [CrossRef]
19. Kumar, M.; Ando, Y. Chemical Vapor Deposition of Carbon Nanotubes: A Review on Growth Mechanism and Mass Production. *J. Nanosci. Nanotechnol.* **2010**, *10*, 3739–3758. [CrossRef]
20. Saito, Y. (Ed.) *Carbon Nanotube and Related Field Emitters*; Wiley-VCH Verlag GmbH & Co. KGaA: Weinheim, Germany, 2010. [CrossRef]

21. Li, H.; Ou, J.P. Smart Concrete, Sensors and Self-Sensing Concrete Structures. *Key Eng. Mater.* **2008**, *400–402*, 69–80. [CrossRef]
22. Jung, M.; Lee, Y.S.; Hong, S.G. Effect of Incident Area Size on Estimation of EMI Shielding Effectiveness for Ultra-High Performance Concrete with Carbon Nanotubes. *IEEE Access* **2019**, *7*, 183105–183117. [CrossRef]
23. Lee, H.; Park, S.; Park, S.; Chung, W. Enhanced detection systems of filling rates using carbon nanotube cement grout. *Nanomaterials* **2020**, *10*, 10. [CrossRef] [PubMed]
24. Çınar, E.; Uygunoğlu, T.; Şimşek, B.; Topçu, İ.B. Effect of carbon black on electrical curing of fresh concrete for cold regions. *Constr. Build. Mater.* **2020**, *247*. [CrossRef]
25. Ahmed, H.I. Behavior of magnetic concrete incorporated with Egyptian nano alumina. *Constr. Build. Mater.* **2017**, *150*, 404–408. [CrossRef]
26. Chuewangkam, N.; Pinitsoontorn, S.; Chindaprasirt, P. Properties of NdFeB magnetic cement. *Cem. Concr. Compos.* **2019**, *103*, 204–212. [CrossRef]
27. He, Y.; Lu, L.; Sun, K.; Wang, F.; Hu, S. Electromagnetic wave absorbing cement-based composite using Nano-Fe3O4 magnetic fluid as absorber. *Cem. Concr. Compos.* **2018**, *92*, 1–6. [CrossRef]
28. Assi, L.; Alsalman, A.; Bianco, D.; Ziehl, P.; El-Khatib, J.; Bayat, M.; Hussein, F.H. Multiwall carbon nanotubes (MWCNTs) dispersion & mechanical effects in OPC mortar & paste: A review. *J. Build. Eng.* **2021**, *43*, 102512. [CrossRef]
29. *ASTM C150/C150M-19a*; Standard Specification for Portland Cement. Book of ASTM Standards. 04.01. ASTM International: West Conshohocken, PA, USA, 2019; pp. 1–10. [CrossRef]
30. Choi, H.; Gong, J.; Lim, Y.; Im, K.H.; Jeon, M. Effects of the electrical conductivity and orientation of silicon substrate on the synthesis of multi-walled carbon nanotubes by thermal chemical vapor deposition. *Nanoscale Res. Lett.* **2013**, *8*, 1–6. [CrossRef]
31. Yoon, H.; Yamashita, M.; Ata, S.; Futaba, D.N.; Yamada, T.; Hata, K. Controlling exfoliation in order to minimize damage during dispersion of long SWCNTs for advanced composites. *Sci. Rep.* **2015**, *4*, 3907. [CrossRef]
32. Prasek, J.; Drbohlavova, J.; Chomoucka, J.; Hubalek, J.; Jasek, O.; Adam, V.; Kizek, R. Methods for carbon nanotubes synthesis—Review. *J. Mater. Chem.* **2011**, *21*, 15872–15884. [CrossRef]
33. Dhillon, G.S.; Kaur, S.; Verma, M.; Brar, S.K. *Biopolymer-Based Nanomaterials: Potential Applications in Bioremediation of Contaminated Wastewaters and Soils*, 1st ed.; Elsevier B.V.: Amsterdam, The Netherlands, 2012. [CrossRef]
34. Saifuddin, N.; Raziah, A.Z.; Junizah, A.R. Carbon nanotubes: A review on structure and their interaction with proteins. *J. Chem.* **2013**, *2013*, 676815. [CrossRef]
35. Bayazit, Ş.S.; Kerkez, Ö. Hexavalent chromium adsorption on superparamagnetic multi-wall carbon nanotubes and activated carbon composites. *Chem. Eng. Res. Des.* **2014**, *92*, 2725–2733. [CrossRef]
36. *ASTM ASTM C642*; Standard Test Method for Density, Absorption, and Voids in Hardened Concrete. Annual Book of ASTM Standards. ASTM International: West Conshohocken, PA, USA, 2013; pp. 1–3.
37. *ASTM C349-08*; Standard Test Method for Compressive Strength of Hydraulic-Cement Mortars (Using Portions of Prisms Broken in Flexure). ASTM International: West Conshohocken, PA, USA, 2008; pp. 1–4.
38. *C1760/1876, A. ASTM Standard C1760*; Standard Test Method for Bulk Electrical Conductivity of Hardened Concrete. ASTM International: West Conshohocken, PA, USA, 2012; pp. 1–5.
39. Hekmatara, H.; Seifi, M.; Forooraghi, K. Microwave absorption property of aligned MWCNT/Fe_3O_4. *J. Magn. Magn. Mater.* **2013**, *346*, 186–191. [CrossRef]
40. Jiao, Z.; Qiu, J. Microwave absorption performance of iron oxide/multiwalled carbon nanotubes nanohybrids prepared by electrostatic attraction. *J. Mater. Sci.* **2018**, *53*, 3640–3646. [CrossRef]
41. Nas, M.S.; Kuyuldar, E.; Demirkan, B.; Calimli, M.H.; Demirbaş, O.; Sen, F. Magnetic nanocomposites decorated on multiwalled carbon nanotube for removal of Maxilon Blue 5G using the sono-Fenton method. *Sci. Rep.* **2019**, *9*, 10850. [CrossRef]
42. Tolba, A.; Gar Alalm, M.; Elsamadony, M.; Mostafa, A.; Afify, H.; Dionysiou, D.D. Modeling and optimization of heterogeneous Fenton-like and photo-Fenton processes using reusable Fe3O4-MWCNTs. *Process Saf. Environ. Prot.* **2019**, *128*, 273–283. [CrossRef]
43. Reddy, P.N.; Kavyateja, B.V.; Jindal, B.B. Structural health monitoring methods, dispersion of fibers, micro and macro structural properties, sensing, and mechanical properties of self-sensing concrete—A review. *Struct. Concr.* **2021**, *22*, 793–805. [CrossRef]
44. Florez, R.; Colorado, H.A.; Alajo, A.; Giraldo, C.H.C. The material characterization and gamma attenuation properties of Portland cement-Fe_3O_4 composites for potential dry cask applications. *Prog. Nucl. Energy* **2019**, *111*, 65–73. [CrossRef]
45. Gao, F.; Tian, W.; Cheng, X. Investigation of moisture migration of MWCNTs concrete after different heating-cooling process by LF-NMR. *Constr. Build. Mater.* **2021**, *288*, 123146. [CrossRef]
46. Jiao, D.; Lesage, K.; Yardimci, M.Y.; El Cheikh, K.; Shi, C.; De Schutter, G. Rheological behavior of cement paste with nano-Fe_3O_4 under magnetic field: Magneto-rheological responses and conceptual calculations. *Cem. Concr. Compos.* **2021**, *120*, 104035. [CrossRef]
47. Cwirzen, A.; Habermehl-Cwirzen, K.; Penttala, V. Surface decoration of carbon nanotubes and mechanical properties of cement/carbon nanotube composites. *Adv. Cem. Res.* **2008**, *20*, 65–73. [CrossRef]
48. Xu, S.; Liu, J.; Li, Q. Mechanical properties and microstructure of multi-walled carbon nanotube-reinforced cement paste. *Constr. Build. Mater.* **2015**, *76*, 16–23. [CrossRef]
49. Roussel, N.; Ovarlez, G.; Garrault, S.; Brumaud, C. The origins of thixotropy of fresh cement pastes. *Cem. Concr. Res.* **2012**, *42*, 148–157. [CrossRef]

50. Madhavi, T.C.; Pavithra, P.; Singh, S.B.; Raj, S.V.; Paul, S. Effect of Multiwalled Carbon Nanotubes On Mechanical Properties of Concrete. *Int. J. Sci. Res.* **2012**, *2*, 166–168. [CrossRef]
51. Sikora, P.; Horszczaruk, E.; Cendrowski, K.; Mijowska, E. The Influence of Nano-Fe_3O_4 on the Microstructure and Mechanical Properties of Cementitious Composites. *Nanoscale Res. Lett.* **2016**, *11*, 182. [CrossRef] [PubMed]
52. Kasuya, T. Electrical Resistance of Ferromagnetic Metals. *Prog. Theor. Phys.* **1956**, *16*, 58–63. [CrossRef]
53. Goodings, D.A. Electrical Resistivity of Ferromagnetic Metals at Low Temperatures. *Phys. Rev.* **1963**, *132*, 542–558. [CrossRef]
54. Heaney, M.B. Electrical conductivity and resistivity. *Electr. Meas. Signal Process. Disp.* **2003**, *1983*, 7-1–7-14. [CrossRef]
55. García, Á.; Schlangen, E.; van de Ven, M.; Liu, Q. Electrical conductivity of asphalt mortar containing conductive fibers and fillers. *Constr. Build. Mater.* **2009**, *23*, 3175–3181. [CrossRef]
56. Le, J.-L.; Du, H.; Dai Pang, S. Use of 2D Graphene Nanoplatelets (GNP) in cement composites for structural health evaluation. *Compos. Part B Eng.* **2014**, *67*, 555–563. [CrossRef]
57. Chacko, R.M.; Banthia, N.; Mufti, A.A. Carbon-fiber-reinforced cement-based sensors. *Can. J. Civ. Eng.* **2007**, *34*, 284–290. [CrossRef]
58. Wen, S.; Chung, D.D.L. A comparative study of steel-and carbon-fibre cement as piezoresistive strain sensors. *Adv. Cem. Res.* **2003**, *15*, 119–128. [CrossRef]
59. Lübeck, A.; Gastaldini, A.L.G.; Barin, D.S.; Siqueira, H.C. Compressive strength and electrical properties of concrete with white Portland cement and blast-furnace slag. *Cem. Concr. Compos.* **2012**, *34*, 392–399. [CrossRef]
60. Lavagna, L.; Musso, S.; Ferro, G.; Pavese, M. Cement-based composites containing functionalized carbon fibers. *Cem. Concr. Compos.* **2018**, *88*, 165–171. [CrossRef]
61. Solís-Carcaño, R.; Moreno, E.I. Evaluation of concrete made with crushed limestone aggregate based on ultrasonic pulse velocity. *Constr. Build. Mater.* **2008**, *22*, 1225–1231. [CrossRef]
62. Güneyli, H.; Karahan, S.; Güneyli, A.; Yapıcı, N. Water content and temperature effect on ultrasonic pulse velocity of concrete. *Russ. J. Nondestruct. Test.* **2017**, *53*, 159–166. [CrossRef]
63. Zhang, J.; Ju, S.; Jiang, D.; Peng, H.-X. Reducing dispersity of mechanical properties of carbon fiber/epoxy composites by introducing multi-walled carbon nanotubes. *Compos. Part B Eng.* **2013**, *54*, 371–376. [CrossRef]

Disclaimer/Publisher's Note: The statements, opinions and data contained in all publications are solely those of the individual author(s) and contributor(s) and not of MDPI and/or the editor(s). MDPI and/or the editor(s) disclaim responsibility for any injury to people or property resulting from any ideas, methods, instructions or products referred to in the content.